Marine Geology 272 (2010) 154–169

Contents lists available at ScienceDirect

Marine Geology

journal homepage: www.elsevier.com/locate/margeo

Acoustic and visual characterisation of methane-rich seabed seeps at Omakere Ridge on the Hikurangi Margin, New Zealand

A.T. Jones [a,*], J. Greinert [b,c], D.A. Bowden [d], I. Klaucke [e], C.J. Petersen [e,f], G.L. Netzeband [e,f], W. Weinrebe [e]

[a] Geoscience Australia, GPO Box 378, Canberra, ACT, 2601, Australia
[b] Renard Centre of Marine Geology, University Gent, Belgium
[c] Royal Netherlands Institute for Sea Research (NIOZ), P.O. Box 59, 1790 AB, Den Burg (Texel), The Netherlands
[d] National Institute of Water and Atmospheric Research, Private Bag 14 901, Kilbirnie, Wellington, New Zealand
[e] IFM-GEOMAR, Wischhofstraβe 1-3, 24148 Kiel, Germany
[f] RWE Dea, Überseering 40, 22297 Hamburg, Germany

ARTICLE INFO

Article history:
Received 8 August 2008
Received in revised form 25 February 2009
Accepted 8 March 2009
Available online 24 March 2009

Keywords:
methane seeps
cold-water reef
Omakere Ridge
Hikurangi Margin
New Zealand
sidescan
seep-related biota

ABSTRACT

Six active methane seeps and one cold-water reef that may represent a relict seep were mapped at Omakere Ridge on New Zealand's Hikurangi Margin during cruises SO191 and TAN0616. Hydroacoustic flares, interpreted to be bubbles of methane rising through the water column were identified in the area. The seep sites and the cold-water reef were characterised by regions of high backscatter intensity on sidescan sonar records, or moderate backscatter intensity where the seep was located directly below the path of the sidescan towfish. The majority of sites appear as elevated features (2–4 m) in multibeam swath data. Gas blanking and acoustic turbidity were observed in sub-bottom profiles through the sites. A seismic section across two of the sites (Bear's Paw and LM-9) shows a BSR suggesting the presence of gas hydrate as well as spots of high amplitudes underneath and above the BSR indicating free gas. All sites were ground truthed with underwater video observations, which showed the acoustic features to represent authigenic carbonate rock structures. Live chemosynthetic biotic assemblages, including siboglinid tube worms, vesicomyid clams, bathymodiolin mussels, and bacterial mats, were observed at the seeps. Cold-water corals were the most conspicuous biota of the cold-water reef but widespread vesicomyid clam shells indicated past seep activity at all sites. The correlation between strong backscatter features in sidescan sonar images and seep-related seabed features is a powerful tool for seep exploration, but differentiating the acoustic features as either modern or relict seeps requires judicial analysis and is most effective when supported by visual observations.

1. Introduction

Seabed fluid flow is of fundamental importance to the marine environment and consequently influences the working of our planet (Judd and Hovland, 2007). It can occur in a variety of forms, and is widespread and dynamic. Although seabed fluid flow is essentially a geological process, it affects marine ecology, ocean chemistry, and the composition of the atmosphere (Kvenvolden and Rogers, 2005). Among the most widely documented seeping fluids are thermogenic hydrocarbons, in the form of natural gas, crude oil, and bitumens (Wilson et al., 1974; Judd and Hovland, 2007). Therefore, seeps can influence atmospheric concentrations of methane, particularly when the seeps occur in shallow water (<100 m) where gas bubbles can survive a journey to the sea surface without dissolving (Kvenvolden and Rogers, 2005; Schmale et al., 2005; McGinnis et al., 2006). Significant amounts of methane are also sequestered within gas hydrates, the global volumes of which vary with addition and withdrawal of free gas over geological time (Kvenvolden, 1988). Additionally, seabed fluid flow influences the composition of sediment pore water and the overlying water column, adding nutrients and substrates that can be oxidised by microbes and thus contributing to biological productivity (Kennicut et al., 1985).

Understanding the dynamics and distribution of seabed fluid flow, particularly of methane, is critical given the widespread, influential nature of the process. Marine geohazards may occur in association with shallow gas, including slope failures and drilling hazards (Hovland and Gudmestad, 2001). The energy potential of gas hydrates has encouraged significant research programmes (Max, 2000), and the oil industry makes use of seeps in petroleum exploration (Abrams, 2005). A more recent concern to marine science is the vulnerability of benthic ecosystems associated with methane seepage (Judd and Hovland, 2007).

Among the most effective tools for characterising seep sites are multibeam and sidescan sonar, which map the morphology and acoustic backscatter of the seafloor, detecting hardness contrasts between unconsolidated sediments and methane-derived authigenic carbonates, chemosynthetic 'cold seep' communities, water column

* Corresponding author. Tel.: +61 2 6249 9768.
E-mail address: Andrew.Jones@ga.gov.au (A.T. Jones).

0025-3227/$ – see front matter.
doi:10.1016/j.margeo.2009.03.008

bubbles, or gas hydrates in the sediment (Orange et al., 2002; Niemann et al., 2005; Holland et al., 2006; Klaucke et al., 2006; Rollet et al., 2006; Naudts et al., 2008).

In this paper, we describe five seep sites and one cold-water reef with associated seepage on the mid-slope Omakere Ridge (Fig. 1) off Hawke Bay, New Zealand. Four of the seep sites (*Kea*, *Kaka*, *Kakapo*, and *Bear's Paw*) and the reef (*Moa*) are previously undocumented seabed features which were discovered at the southern end of Omakere Ridge where it bifurcates into parallel ridgelines. All of these sites, plus Lewis and Marshall's (1996) LM-9 site, are located towards the crests of the two ridgelines in approximately 1100–1170 m water depth. The data presented here were acquired during the course of two marine surveys: firstly the RENEWZ-1 NOAA-NIWA New Zeeps voyage (TAN0616) in November 2006, and then an IFM-GEOMAR survey aboard the RV SONNE (SO191) between January and March 2007. In this study, the seepage sites are characterised on the basis of sidescan sonar and multibeam swath data. Indicators of shallow gas in the region are also described in sub-bottom profile (SBP) data. Ground truthing of the seep sites was undertaken with underwater video and still cameras. The spatial relationship between high acoustic backscatter features in the sidescan sonar data and seabed characterisation from continuous underwater video observations is analysed quantitatively in a geographic information system (GIS). Our data and results suggest that seabed signatures of seepage can be identified with varying degrees of confidence depending on their morphology, but that definitive identification of modern seeps may require visual observations.

2. Study area

The Hikurangi Margin, off the east coast of New Zealand's North Island, is part of the Kermadec-Hikurangi subduction zone, which is a component of the boundary between the Pacific and Australian tectonic plates. The style of subduction tectonics varies along the

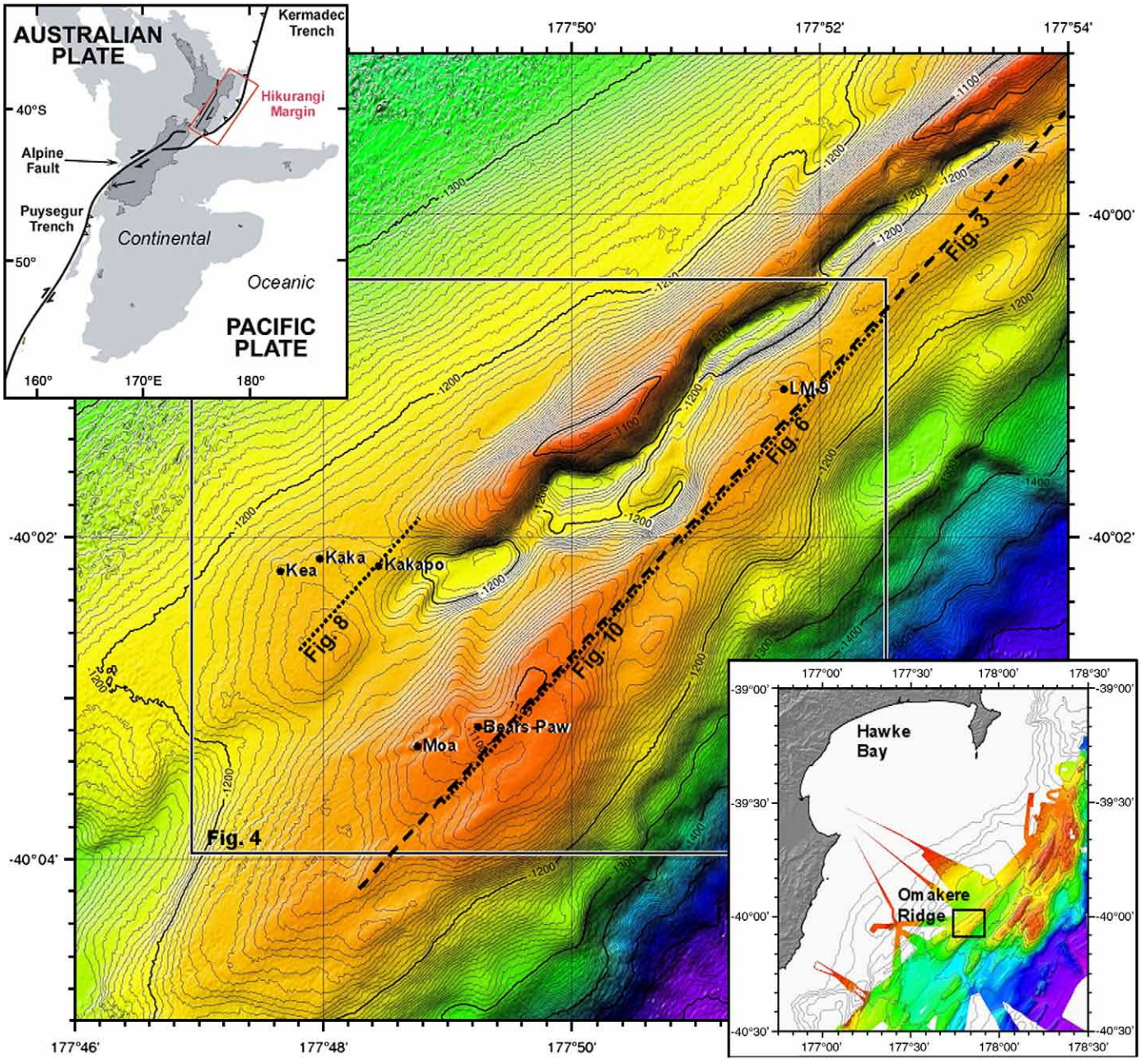

Fig. 1. Location and bathymetry of Omakere Ridge, including the location of seep sites described in this study.

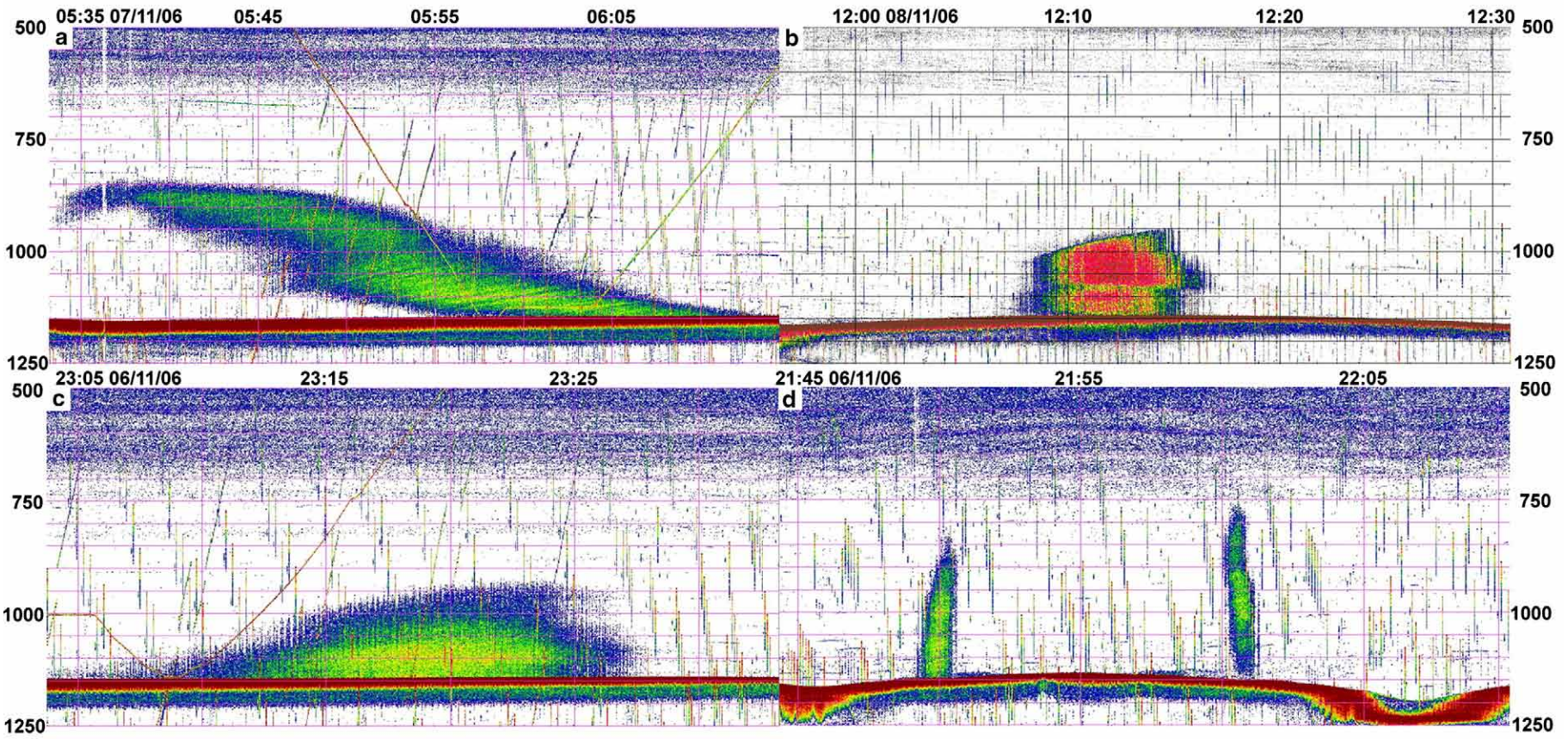

Fig. 2. Hydroacoustic flares from RENEWZ-1 NOAA-NIWA New Zeeps voyage TAN0616 imaging methane seepage at the LM-9 site (*y*-axis is depth in meters, *x*-axis is time of transect). Vessel speed: a,b) <1 kn, c) 3 kn, d) 6 kn.

Hikurangi Margin from predominantly strike-slip in the south, to accretion in the centre, to tectonic erosion responding to subducting seamounts in the north. Omakere Ridge, the focus of this study, is one of a series of prominent northeast–southwest orientated anticlinal ridges associated with major thrust faults on the actively accreting part of the Hikurangi Margin. Details of the tectonic setting of the Hikurangi Margin are given in Barnes et al. (2010-this issue).

Natural hydrocarbon seeps on the Hikurangi Margin were first investigated by Lewis and Marshall (1996), who described methane-derived authigenic carbonate, chemoautotrophic clams, and hydro-acoustic flares from thirteen sites around New Zealand. Acoustic flares reported by fishermen at the LM-9 site (Fig. 1) were cited as evidence of seepage at Omakere Ridge (Lewis and Marshall, 1996), although dredging of the site in June 1994 failed to collect any seep-associated biota. The Hikurangi Margin is also known for the occurrence of a widespread, strong bottom simulating reflection (BSR), interpreted to be the base of a gas hydrate zone underlain by widespread free gas (Henrys et al., 2003). The previously mapped extent of this BSR included a single transect that intersected Omakere Ridge (Henrys et al., 2003). A more comprehensive discussion of previous work on cold seeps and hydrates on the Hikurangi Margin is given in Greinert et al. (2010-this issue).

During RV TANGAROA survey TAN0616, imaging of hydroacoustic flares over the LM-9 site on Omakere Ridge (Fig. 2) confirmed that the seep that was active in the mid-90's (Lewis and Marshall, 1996) was still bubbling. Seeping methane was also detected at anomalous water column concentrations (up to 165 nM) over Omakere Ridge in gas chromatography (GC) based analyses of sampled water from CTD casts on TAN0607 (RV TANGAROA, June 2006; see Greinert et al., 2010-this issue, for details) and SO191. High methane concentrations were recorded over the Bear's Paw site hundreds of meters above the seafloor, but only slightly increased concentrations (<40 nM) were observed over LM-9 during TAN0607 and SO191. More details of free and dissolved methane in the water column over the Hikurangi Margin are presented in Faure et al. (2010-this issue).

Multi-channel seismic (MCS) data acquired during SO191 with a 4-channel streamer of 36 m active length and a single GI-Gun source with a volume of 250/105 in^3 (see Netzeband et al., 2010-this issue, for details on the acquisition and processing of MCS from SO191) show a distinct BSR underlying Omakere Ridge (Fig. 3), suggesting that the base of the gas hydrate zone described by Henrys et al. (2003) for the broader Hikurangi Margin extends along the length of the ridge. This interpretation is supported by the negative polarity of the reflection, indicating a transition from higher seismic velocity (possible gas hydrate cementation) to lower seismic velocity below (free gas).

3. Methods

A wide range of reconnaissance surveying and seabed sampling techniques were applied to studying the cold seeps of the Hikurangi Margin during TAN0616 and SO191 (Greinert et al., 2010-this issue). This study focuses on the characterisation of the Omakere Ridge seep sites with sidescan and multibeam swath sonar, SBP and visual observations from underwater video.

Sidescan sonar data were obtained with the digital, deep-towed DTS-1 system operated by IFM-GEOMAR. The DTS-1 is a modified EdgeTech dual frequency chirp system working with 75 and 410 kHz centre frequencies for maximum ranges of 750 and 150 m, respectively. Data presented herein are from the 75 kHz signal, which is a 14 ms long pulse of 7.5 kHz bandwidth providing an across-track resolution of 5.6 cm. Towing speed averaged 2.5 kn and the data have been processed for a pixel size of 2 m using the PRISM package from Southampton Oceanography Centre (Le Bas et al., 1995). High back-scatter regions are presented as light features in the sidescan data. The DTS-1 also includes EdgeTech's Chirp SBP DW-216. The chirp SBP system was operated in a frequency range of 2–10 kHz. The data

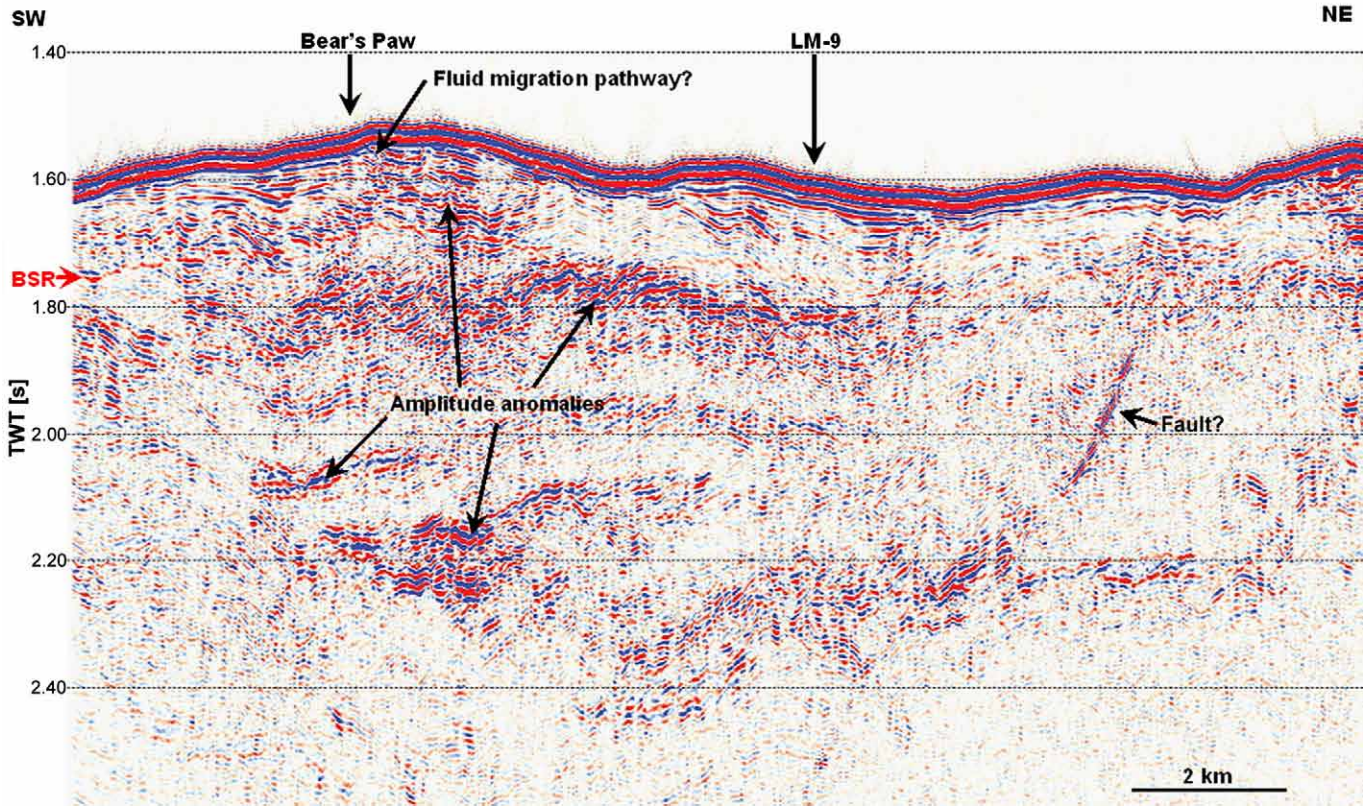

Fig. 3. Multi-channel seismic profile through Omakere Ridge showing a distinct bottom simulating reflection interpreted to be a hydrate/free gas interface, potential amplitude anomalies and a potential vertical migration pathway. Profile location shown in Fig. 1.

shown represent the envelope of the dechirped recorded data and are corrected for geometric spreading. A sub-bottom penetration of up to 50 m and a vertical resolution of approximately 1 m were achieved. An ultra short baseline (USBL) navigation system provided exact navigation of the towfish resulting in a position accuracy of 10–20 m. Additionally, a depth sensor was mounted on the towfish to ensure accurate depth readings. Thus, a reliable depth correction of the deep-towed SBP profiles to the true seafloor morphology could be achieved in processing.

Photographic observations of the seabed were made using two towed camera platforms: NIWA's Deep Towed Imaging system (DTIS) during TAN0616, and the RV SONNE's Ocean Floor Observation System (OFOS) during SO191. Both platforms incorporate vertically orientated colour digital video cameras and digital stills cameras, with paired parallel red lasers for image scale. Camera platforms were towed at approximately 2 m above the seabed at speeds <0.5 ms^{-1} and recorded continuous video footage with digital still images taken at 15 s intervals throughout each deployment. The seabed position of the camera was tracked by means of USBL acoustic positioning systems (Simrad HPR and Ixsea Poseidonia). Transects were planned, and spatially referenced observations were recorded in real time, by means of the Ocean Floor Observation Protocol software (OFOP; Huetten and Greinert, 2008) which allows ship and camera positions to be monitored against georeferenced acoustic images of the seabed.

Post-voyage video analyses were run using OFOP. Raw USBL position data were first smoothed using a 21 point running average. The smoothed tracks were then used as the basis for generating splined seabed tracks with positions at 1 s intervals. These tracks were synchronised with the video files (in MPEG or AVI format) and the transects were rerun under controlled conditions with pause, replay, and slow-motion facilities. Observations were allocated to three substratum categories and one biota category (Table 1). Because the primary aim of the surveys was to identify areas of active methane seepage and authigenic carbonate rock formation, substratum observation categories were designed to highlight the occurrence of seep-associated features. Seep sites were characterised by isolated areas of carbonate rock structures in extensive plains of soft, muddy sediments. Therefore, a simplified hierarchy of substratum descriptors was used in which the highest level category 'seabed_a' distinguished simply between muddy sediments and the presence of any hard substrata, without attempting to estimate relative coverage of different substrata. Thus, an observation of 'Carbonate' within the category 'seabed_a' indicates only that rock of some sort was visible, even if it constituted only a small proportion of the field of view, whereas 'Muddy sediments' indicates 100% cover by soft sediments. Subsequent categories refine this coarse level distinction and all observation types used, together with their working definitions, are set out in Table 1. Note that the full range of observation descriptors available during video analysis was considerably greater than this but the subset presented here was condensed out of the full analyses as being the most commonly used and most relevant to the present analysis.

In practice, observations were recorded as a single time-referenced stream during video playback. However, because the categories 'seabed_a', 'seabed_b', and 'relief' were treated as continuous descriptors using a 'fill-down' treatment (Table 1) and pause and rerun facilities were available during video playback, the logging technique allowed multiple observations at any one time increment. A spatially-enabled database was constructed using PostgreSQL/PostGIS (www.postgresql.org, http://postgis.refractions.net) with embedded scripts to allocate observations within each category to separate database fields and to fill down at 1 s intervals those which represent continuous substrata (Table 1). This database was then interrogated using the open source GIS application Quantum GIS (www.qgis.org) from which shapefiles of the video observations were exported to ArcGIS v 9.2 (www.esri.com) for analysis in relation to georeferenced sidescan sonar images of the area. Greyscale values representing backscatter intensity were then extracted from the sidescan raster image for polygons identified by video ground truthing as representing particular seabed types.

4. Acoustic characterisation

The seep and reef sites on Omakere Ridge were all characterised by elevated and heterogeneous backscatter intensity on sidescan sonar

Table 1
Hierarchy of substratum descriptors used to classify underwater video observations over Omakere Ridge.

Category	Treatment	Observation	Description	Modifiers
Seabed_a	Fill down	Carbonate	Presence of any rock substratum	→Seabed_b →Relief, →Seabed_c →Biota
		Muddy sediment	100% cover muddy sediments	→Seabed_c →Biota
Seabed_b	Fill down	Outcrop	Continuous authigenic carbonate rock structures without chemosynthetic fauna	→Relief, →Seabed_c →Biota
		Chemoherm	Continuous authigenic carbonate structures with live chemosynthetic fauna	→Relief, →Seabed_c →Biota
		Boulders	Discrete pieces of carbonate rock >25 cm across visible above mud overlay	→Seabed_c →Biota
		Cobbles	Discrete pieces of carbonate rock <25 cm across visible above mud overlay.	→Seabed_c →Biota
Relief	Fill down	Low relief	Height estimated as <1 m	
		High relief	Height estimated as >1 m	
		Flat plates	Flat carbonate structures identified primarily by step edges	
Seabed_c	Point observation	Coral rubble	Fragments of cold water stony corals	→Biota
		Shell hash	Unidentifiable shell fragments	→Biota
		Calyptogena sp. shell	Shell valves of *Calytogena* sp. clams	→Biota
		Bathymodiolin shell	Shell valves of bathymodiolin mussels	→Biota
		Sulphidic sediment	Dark sediment usually associated with dense populations of ampharetid polychaete worms	→Biota
Biota	Point observation	Bacterial mat	Live bacterial mat on substratum surface	
		Bathymodiolus sp.	Live Bathymodiolin mussels	
		Calyptogena sp.	Live *Calyptopgena* sp. clams	
		Vestimentiferan	Live *Lamellibrachia* sp siboglinid worms	
		Coral (intact)	Live or structurally intact cold water corals	

Depending on category, observations are treated as either continuous ("Fill down") or point observations. Observations in higher level categories can be modified by simultaneous observations in other categories. For instance, an observation of "Carbonate" under Seabed_a can be modified by observations in all other categories, whereas observations of "Muddy sediment" can only be modified by observations in categories Seabed_c and Biota.

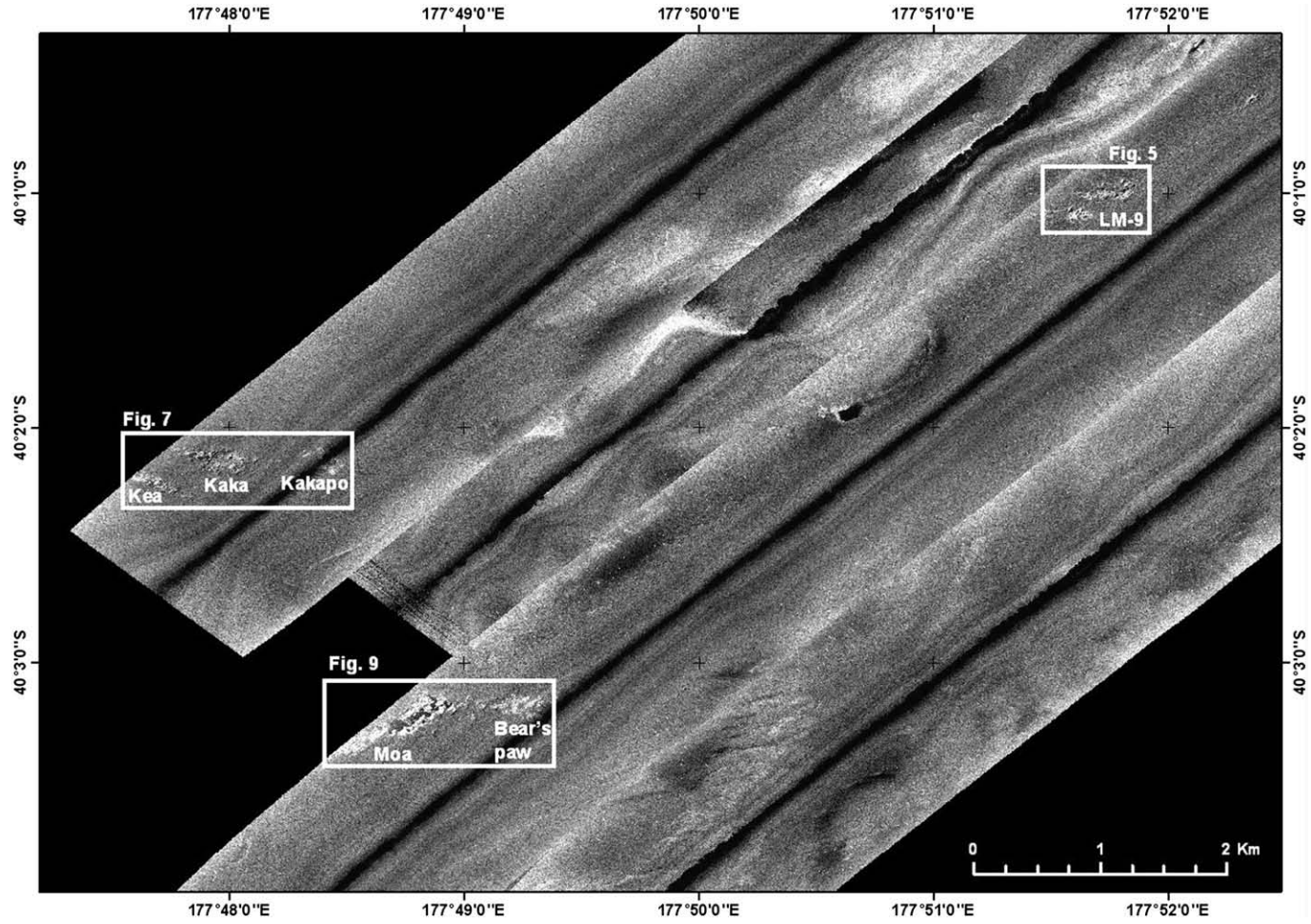

Fig. 4. 75 kHz DTS-1 sidescan sonar mosaic of the southern end of Omakere Ridge, showing the five seep sites (Kea, Kaka, Kakapo, Bear's Paw and LM-9) and cold water reef (Moa) described in this study. The lighter and darker swaths were acquired during alternate legs. Location of mosaic shown in Fig. 1.

mosaics by comparison with surrounding soft sediments (Fig. 4). For the purpose of discussion in this study, the sites (Table 2) are divided into three groups according to their location: the LM-9 area to the northeast centred on 40°1′S and 177°51.67′E, the area to the west around 40°2.15′S and 177°48′E that includes the Kea, Kaka and Kakapo seeps, and the area to the southwest around 40°3.2′S and 177°49′E that includes the Bear's Paw seep and the Moa cold-water reef. No active gas emission in the form of gas bubbles from any seeps sites was observed in the water column of the unprocessed 75 kHz sidescan sonar records (cf. Klaucke et al., 2005).

4.1. LM-9

The single seep site in this area is named LM-9 in recognition of its identification as Site 9 by Lewis and Marshall (1996). The LM-9 seep covers an area of approximately 0.6 km^2 (Table 2), and is characterised by a region of moderate backscatter intensity on sidescan sonar records (Fig. 5). The seep comprises two slightly disparate regions on the seabed; a larger and more irregularly-shaped area of moderate backscatter intensity to the northeast, and a smaller oblate-shaped area of higher backscatter intensity to the southwest. The sidescan

Table 2
Location of methane seeps and a cold-water reef on Omakere Ridge.

Name	Latitude	Longitude	Water depth	Area	Nature	Video transects
LM-9	40°1S	177°51.67E	1150 m	0.6 km^2	Seep site	TAN0616-044 TAN0616-055 TAN0616-056
Kea	40°2.23S	177°47.67E	1170 m	0.3 km^2	Seep site	SO191-2-OFOS-3 SO191-2-OFOS-6 SO191-2-OFOS-17
Kaka	40°2.1S	177°47.95E	1170 m	0.7 km^2	Seep site	SO191-2-OFOS-3 SO191-2-OFOS-6 SO191-2-OFOS-17
Kakapo	40°2.12S	177°48.42E	1165 m	0.3 km^2	Seep site	SO191-2-OFOS-6
Bear's Paw	40°3.17S	177°49.25E	1100 m	0.5 km^2	Seep site	SO191-2-OFOS-7
Moa	40°3.23S	177°48.75E	1120 m	1.1 km^2	Cold water reef	SO191-2-OFOS-7 SO191-2-OFOS-16

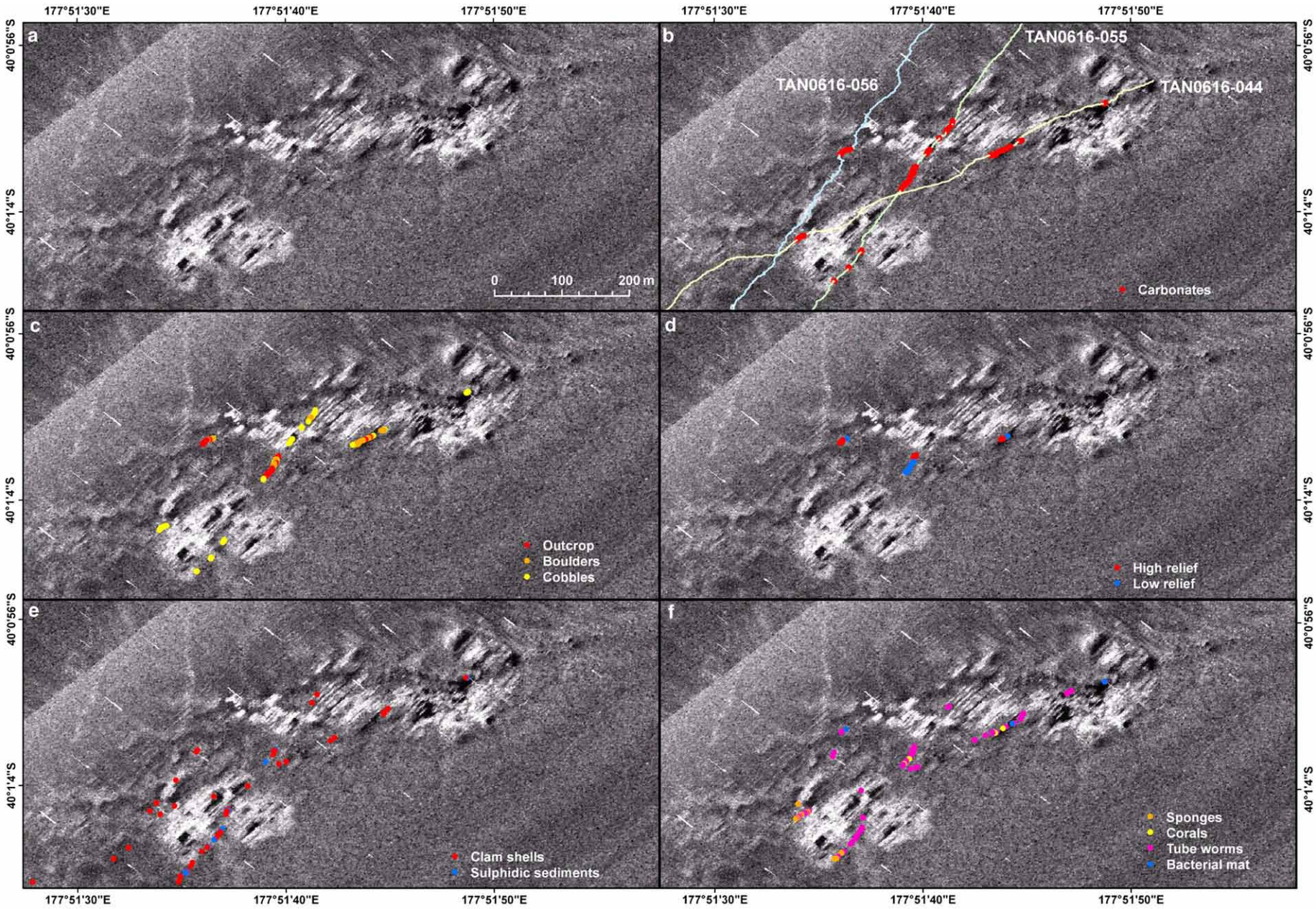

Fig. 5. a) Sidescan sonar image of the LM-9 seep. b) Differentiation of muddy sediments and carbonates in underwater video transects. c) Characterisation of the type of seabed carbonate. d) Relative relief of carbonate outcrop. e) Biogenic substrata and sulphidic sediments. f) Seep related fauna biota. Location of image shown in Fig. 4.

sonar signatures of this seep do not display well-developed acoustic shadows (low backscatter intensity—dark features) despite being in the far range of the sidescan swath, which suggests that the topography of the seeps is of low relief.

Chirp SBP data acquired on a southwest–northeast orientated transect approximately 450 m to the southeast of LM-9 (Fig. 1) display a distinct zone of decreased signal intensity less than 400 m to the southwest of the seep site (Fig. 6). The lack of signal intensity in this zone is interpreted to represent gas blanking, where gas within the shallow sedimentary section absorbs the transmitted acoustic power. This shallow gas front may represent the migration pathway of the methane as it migrates from the hydrate/free gas boundary (Fig. 3) to the seep site at LM-9.

4.2. Kea/Kaka/Kakapo

Kea and Kakapo seeps both cover areas of approximately 0.3 km^2, whereas the Kaka seep is the largest of the seep sites on Omakere Ridge, occupying an area of approximately 0.7 km^2 (Table 2). All three seep sites, particularly Kea, are elongate in a NNW–SSE orientation, although Kaka has an indented southern margin and forms a horseshoe-like shape (Fig. 7). All are characterised by a region of high backscatter intensity on sidescan sonar records, although the signature varies between sites. The Kea and Kaka sites consist of scattered high backscatter regions with well developed acoustic shadows, which are indicative of relatively high topographic relief, but these are interspersed with areas of lower backscatter at background levels. The Kakapo site is a region of moderate backscatter intensity without acoustic shadows. However, the sidescan signature of the Kakapo site cannot be considered diagnostic as it lies directly below the path of the towfish, and sidescan is most effective at measuring backscatter contrasts in the middle to far range of the data swath.

Chirp SBP data acquired on a southwest–northeast orientated transect directly through the Kakapo seep, and approximately 370 and 270 m to the southeast of the Kea and Kaka seeps, respectively, display an irregular zone of increased signal intensity directly below the Kakapo seep site (Fig. 8). The zone of increased signal intensity, which does not conform to the near-surface strata, is interpreted to represent acoustic turbidity, where gas bubbles within the shallow sedimentary section reflect the transmitted acoustic power. The zone of acoustic turbidity intersects the sea surface directly below the Kakapo seep, which very strongly suggests that this shallow gas front represents the migration pathway of the methane as it migrates from the hydrate/free gas boundary (Fig. 3) to the seep site.

4.3. Moa/Bear's Paw

There are two seabed features in this area: a seep site named Bear's Paw, and a cold-water reef (see Section 6) named Moa which has seep areas at its southwestern end. The Bear's Paw seep covers an area of approximately 0.5 km^2, whereas the Moa cold-water reef and seep occupies an area of approximately 1.1 km^2 (Table 2) and is elongate in a northeast–southwest orientation (Fig. 9). Both sites are characterised by high backscatter intensity on sidescan sonar records, but the characteristics of their acoustic signatures differ. The main part of the Moa site consists of a region with very high backscatter associated with well developed acoustic shadows, which is indicative of high and steep topographic relief. Towards the southwestern end, however, while backscatter intensity is still high, there is no evidence of the pronounced shadowing. The Bear's Paw site, by contrast, consists entirely of moderate backscatter intensity without acoustic shadows, indicating lower relief.

Chirp SBP data acquired on a southwest–northeast orientated transect approximately 70 and 450 m to the southeast of the Bear's Paw seep and Moa cold-water reef, respectively, displays some irregular zones of increased signal intensity from 400 m to 2 km to the northeast of the Bear's Paw seep (Fig. 10). As with the Kea, Kaka and Kakapo area, the zone of increased signal intensity is interpreted to represent acoustic turbidity, with gas bubbles within the shallow sedimentary section reflecting the transmitted acoustic power of the SBP system.

5. Morphological characterisation

Multibeam bathymetric mapping undertaken during TAN0616 and SO191 (Greinert et al., 2010-this issue) shows the existence of the seep sites as slightly elevated seabed features (Fig. 11), although the morphological expressions of the three scattered seep occurrences at LM-9 are not as well defined as the other sites. The seep sites are typically 2 to 4 m high, which fits well with the visually observed height of the chemoherm structures. Therefore, in most cases, it would have been possible to map the Omakere Ridge seep sites with multibeam swath data alone. However, without the additional high resolution sidescan information it would have been difficult to accurately and simply pinpoint the seeps. The multibeam data do not have the same spatial resolution as the sidescan data due to integrating over a wider area given by the system-defined beam width. The systems used during the surveys (EM300 and EM120) have a beam width of 2° that results in a footprint width of 41 m in water depths of 1170 m. Nevertheless, the horseshoe-like shape of Kaka is also shown in the bathymetry, with an elevated rim at the high backscatter areas in the sidescan data (Fig. 12).

6. Visual characterisation

6.1. LM-9

In seabed video observations at the LM-9 seep site, carbonate coverage of the seabed was sparse (Fig. 5b). The northern region within the seep consisted predominantly of scattered boulders and cobbles with occasional patches of mainly low relief outcrop (Figs. 5c,d and 13a). Only cobbles of carbonate were observed in the seep's

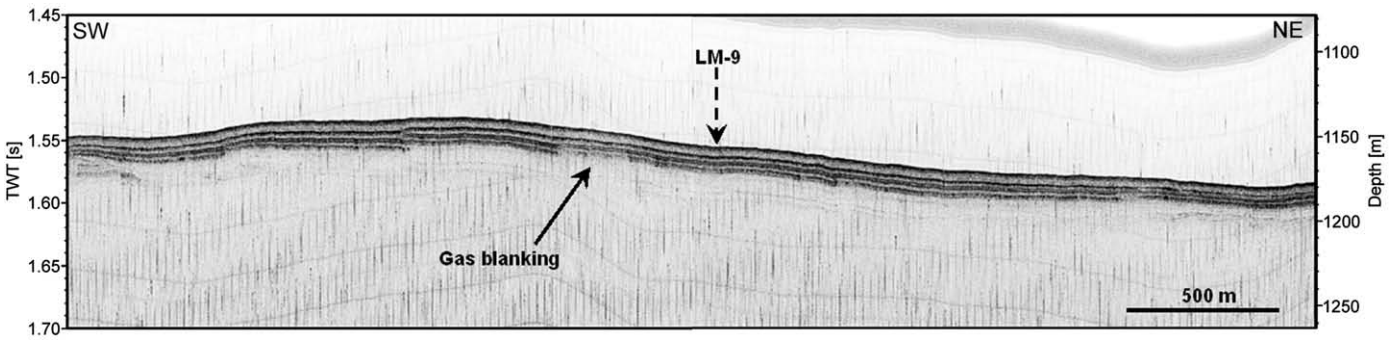

Fig. 6. 2–10 kHz chirp sub-bottom profile across the LM-9 seep. LM-9 is projected onto the profile from 450 m to the northwest. Profile location shown in Fig. 1.

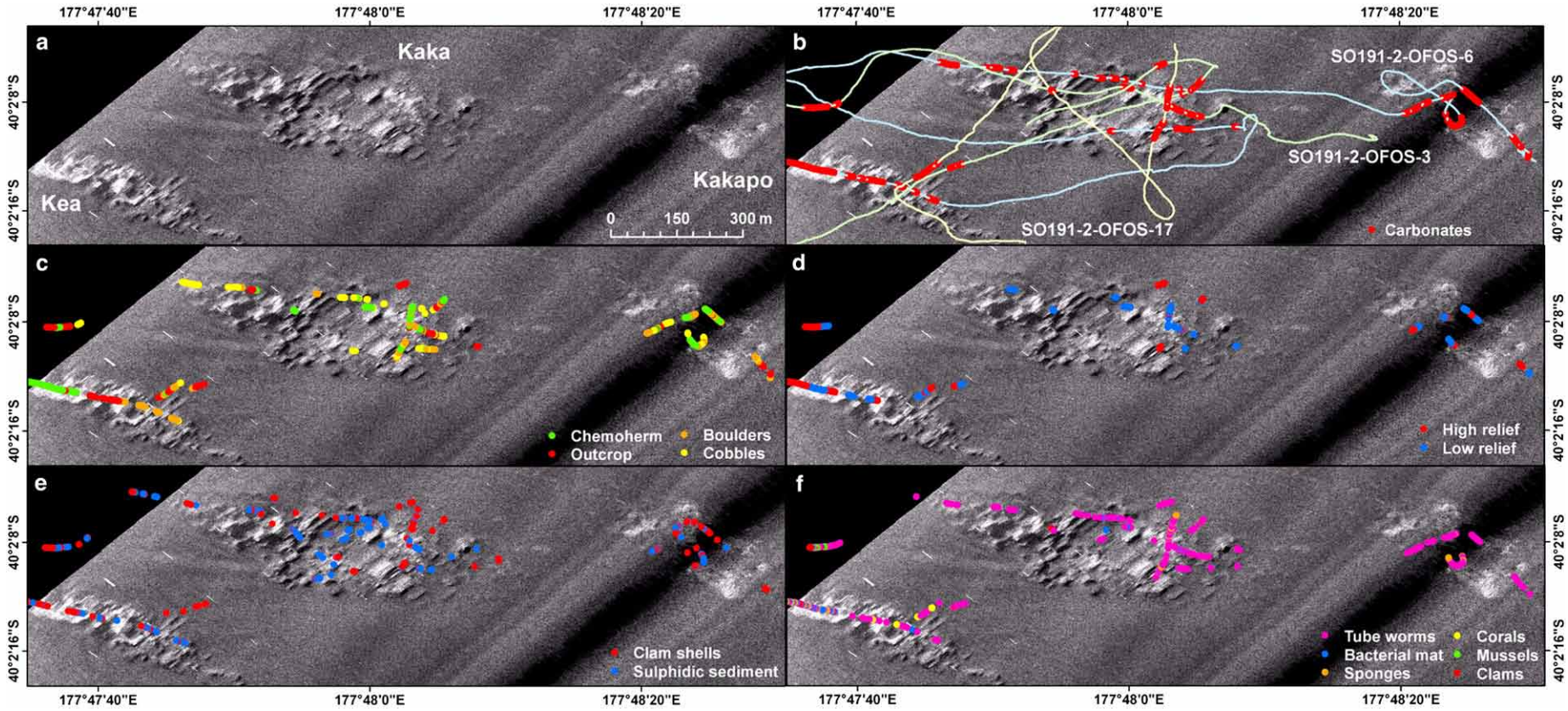

Fig. 7. a) Sidescan sonar image of the Kea, Kaka and Kakapo seeps. b) Differentiation of muddy sediments and carbonates in underwater video transects. c) Characterisation of the type of seabed carbonate. d) Relative relief of carbonate outcrop. e) Biogenic substrata and sulphidic sediments. f) Seep related fauna biota. Location of image shown in Fig. 4.

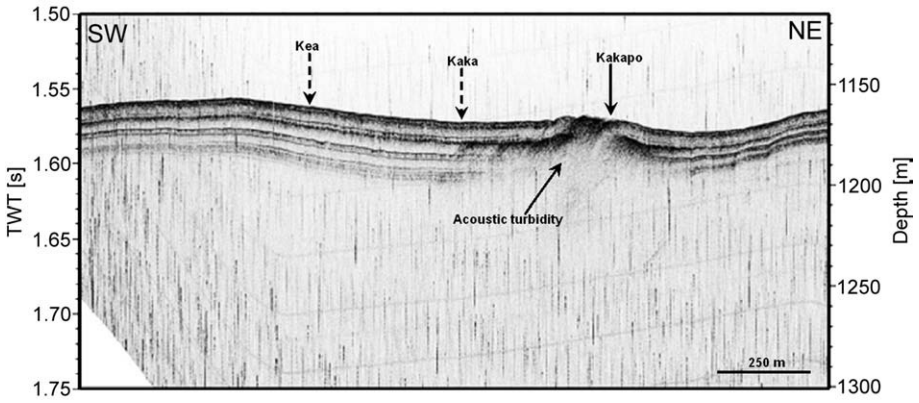

Fig. 8. 2–10 kHz chirp sub-bottom profile across the Kea, Kaka and Kakapo seeps. Kea and Kaka are projected onto the profile from 370 and 270 m to the northwest, respectively. Profile location shown in Fig. 1.

southern region (Fig. 5c). This distribution of carbonate type is inconsistent with the higher backscatter seen in the southern area in the sidescan sonar data (Fig. 5a). It is likely that the carbonates causing the higher backscatter are limited in extent and that the video transects, which encompass a field of view of approximately 2 m at the seabed, missed the main carbonate areas (Fig. 5b).

Shell valves of *Calyptogena* sp. clams were widely distributed in low densities around the southern part of the site, where patches of sulphidic sediments were also seen (Fig. 5e). Living chemosynthetic biota were observed, again in relatively low abundances, in both the northern and southern parts of the seep and were generally associated with patches of low relief carbonate. The fauna consisted almost exclusively of the large siboglinid tube worms *Lamellibrachia* sp., which were observed in all transects (Fig. 5f) together with occasional bacterial mats and, in the southern area only, seep-associated hexactinellid sponges. A few cold water corals were observed on carbonates in the northern region (Fig. 5f).

6.2. Kea/Kaka/Kakapo

Video observations of the Kea, Kaka and Kakapo seeps showed scattered carbonate coverage at each site (Fig. 7b), with outcrops and chemoherms of predominantly low relief (Fig. 7c,d), as well as areas of boulders and cobbles (Fig. 7c). The most abundant seep fauna and extensive areas of chemoherm were seen at the western end of Kea. The visual observations support the acoustic interpretations for the Kakapo seep in that the moderate backscatter (without acoustic shadows) across this site (Fig. 7a) is related more to the position of the seep directly below the path of the side-looking towfish than to any major contrast in seabed character relative to the Kea and Kaka seeps.

Shell valves of *Calyptogena* sp. clams and patches of sulphidic sediment were widely distributed at all three seeps (Figs. 7e and 13b) but were seen generally in low abundance other than in the chemoherm at the western end of Kea. Of the living biota, *Lamellibrachia* sp. tube worms were the most widely distributed, occurring at all three seeps (Figs. 7f and 13c). The chemoherm at the western end of Kea had the highest densities of chemosynthetic fauna and was notable for the presence of *Bathymodiolus* sp. mussels, *Calyptogena* sp. clams, and hexactiellid sponges in addition to tube worms.

6.3. Moa/Bear's Paw

Video observations of the Moa and Bear's Paw sites showed dense carbonate coverage at each site (Fig. 9b) but their characteristics were very different in terms of both geomorphology and fauna. The main part of the Moa site, represented by the areas of very high backscatter intensity in the sidescan images was characterised by steep, high relief, carbonate outcrop colonised in many places by cold water corals (Figs. 9c,d and 13d). Chemoherm habitats with live chemosynthetic fauna were seen only at the southwestern end of the Moa site (Fig. 13e). In contrast, the Bear's Paw site was almost exclusively chemoherm of moderate relief interspersed with areas of sulphidic soft sediments and supporting exceptionally high abundances of chemosynthetic fauna (Fig. 13f). The most conspicuous fauna in both Moa and Bear's Paw chemoherm areas were *Lamellibrachia* sp. tube worms and *Calyptogena* sp. clams (Fig. 13e,f). Sulphidic sediments and shell valves of dead *Calyptogena* sp. clams were widely distributed in and around both the Moa and Bear's Paw sites (Fig. 9e) but shell valves of bathymodiolin mussels were observed only at the Moa site (Fig. 9c,d).

7. Sidescan backscatter in relation to video ground truthing

Visual examination of the sidescan sonar images was used with considerable success as the primary method for identifying the precise location of seep sites during the cruises; therefore there is a direct and intuitively obvious relationship between the characteristics of the backscatter image and the probability of occurrence of seep sites in the study area. In practice, areas which returned high intensity or heterogeneous backscatter by comparison with surrounding regions of uniform backscatter were targeted for further investigation. This is entirely logical in as much as we know that 1) hard substrata return higher backscatter (or more heterogeneous backscatter if significant shadowing occurs) than soft sediments, and 2) hard substrata in the form of carbonate rock develop as a direct consequence of biogeochemical processes at seep sites. Following from this, it is also clear that in cases where there are spatial discrepancies between the sidescan backscatter values and video ground truth observations, the most likely explanation is that there were inaccuracies in determining the seabed position of either the video camera or the sidescan towfish; the former being the most likely in light of the way these tools are deployed.

A thorough statistical treatment of this relationship is beyond the scope of the present study but the observed relationship between backscatter and seabed characteristics is illustrated here by histograms showing the relative frequency of occurrence of greyscale values in the sidescan image for areas identified by video ground truthing as being either seep sites or soft sediment. The histogram for each seep site was generated from pixel values enclosed by a polygon drawn to enclose all video observation points at that site identified as carbonate. For direct comparison with surrounding seabed values, each polygon was then translated along the track of the sidescan swathe (thus avoiding problems associated with differences between near and far field backscatter values) until it entirely overlaid an area of uniform backscatter for which only soft sediment observations had been recorded, and a matching histogram of greyscale values was generated.

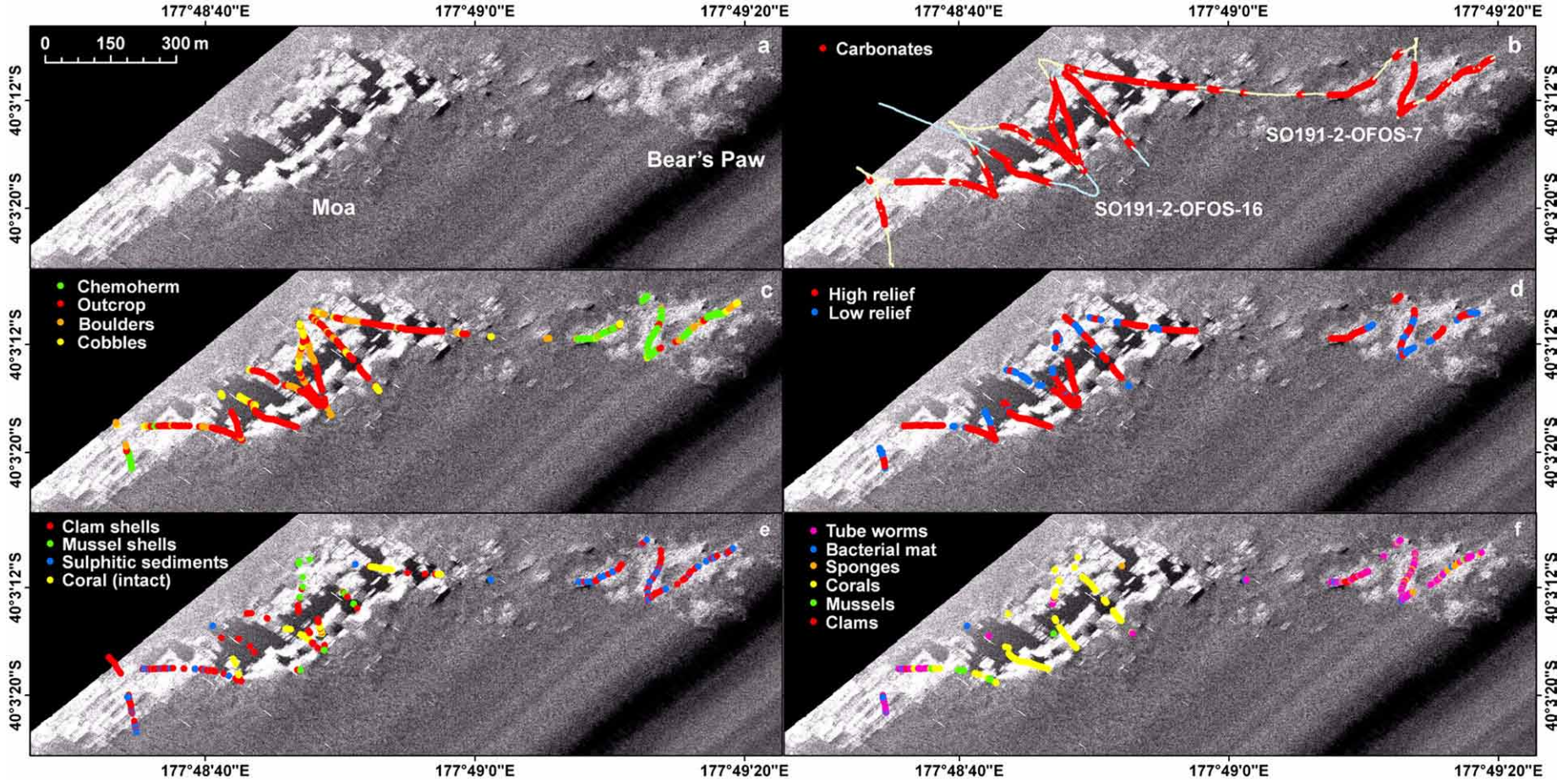

Fig. 9. a) Sidescan sonar image of the Bear's Paw seep and the Moa cold-water reef. b) Differentiation of muddy sediments and carbonates in underwater video transects. c) Characterisation of the type of seabed carbonate. d) Relative relief of carbonate outcrop. e) Biogenic substrata and sulphidic sediments. f) Seep related fauna biota. Location of image shown in Fig. 4.

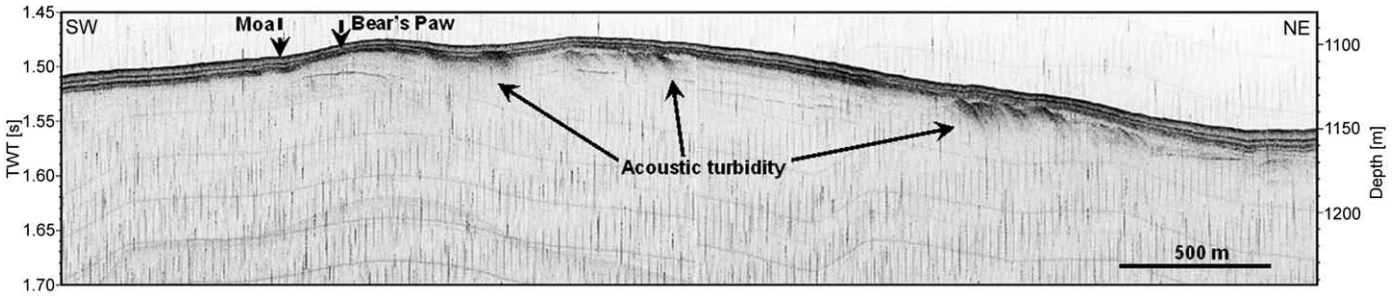

Fig. 10. 2–10 kHz chirp sub-bottom profile across the Bear's Paw and Moa area. Bear's Paw and Moa are projected onto the profile from 70 and 450 m to the northwest, respectively. Profile location shown in Fig. 1.

Three video transects were incorporated into this analysis of the backscatter data: SO191-2-OFOS-6 (Fig. 7b), SO191-2-OFOS-7 and SO191-2-OFOS-16 (Fig. 9b) covering the Kea, Kaka, Kakapo and Bear's Paw seep sites and the Moa cold-water reef and seep (Table 2). These transects were selected because they showed consistent and accurate correlation between observations of seabed morphology and backscatter variations. The remaining transects showed obvious but inconsistent discrepancies that are assumed to be caused by inaccuracies associated with the acoustic positioning systems used (Fig. 7b–d).

Profiles from all sites show that backscatter from the seep areas is characterised by lower kurtosis than adjacent soft sediments, with extended tails in the high backscatter values (Fig. 14). It is interesting that most sites also show extended tails in the low backscatter distribution, which is indicative of the presence of acoustic shadows in areas of high relief. While LM-9, Bear's Paw, Kea, Kaka, and Kakapo show broadly similar backscatter profiles, the histogram for the entire Moa site has very low kurtosis coupled with weak bimodality. In video observations Moa was seen to consist of a large area of high relief cold water reef which was contiguous with an area of lower relief

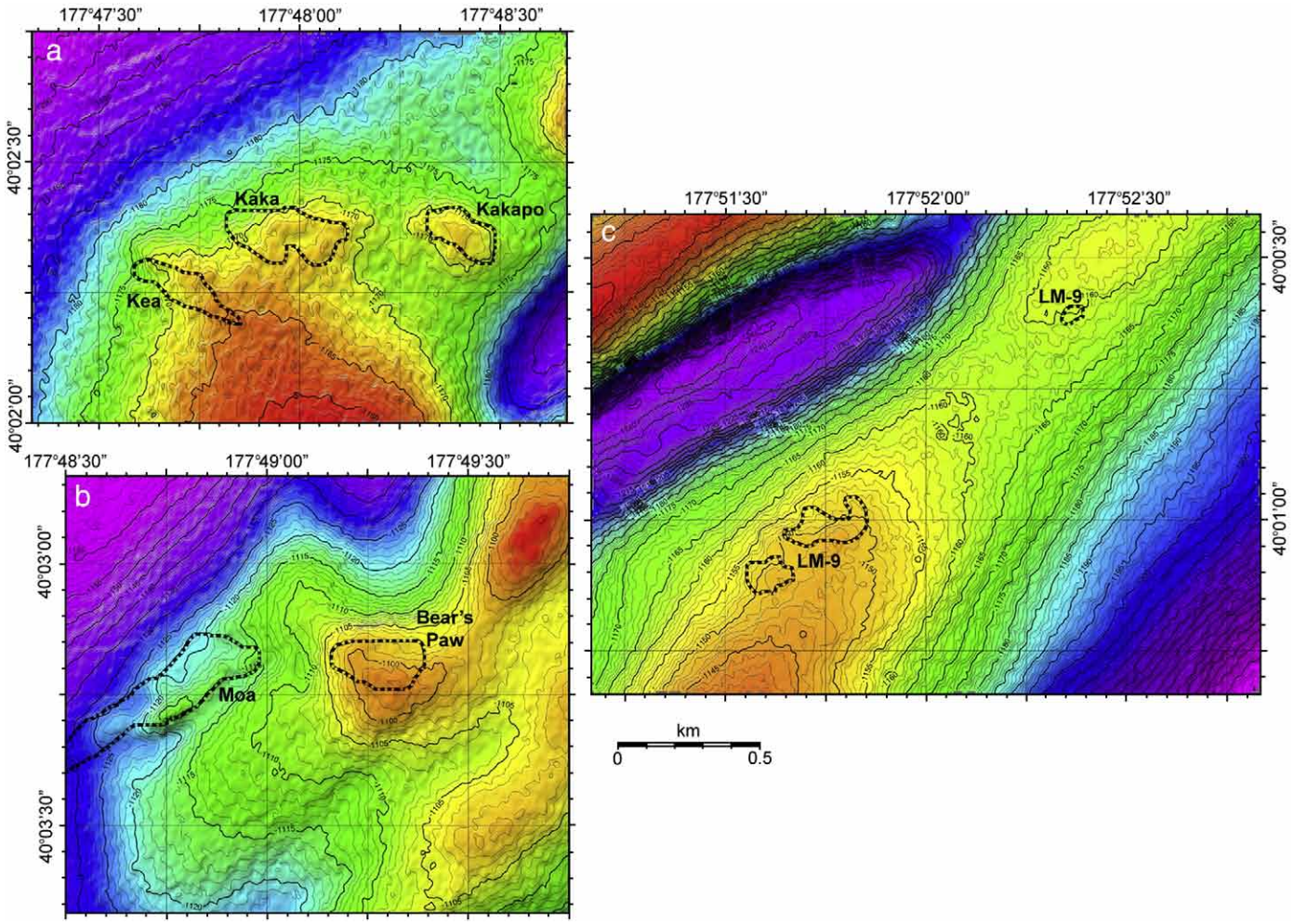

Fig. 11. Detailed bathymetry of the three seep regions at Omakere Ridge. Contour lines in all maps are every meter; the grid size was 15 m which was re-sampled to 7.5 m. Dashed lines are high-backscatter regions from sidescan sonar data. The majority of seeps show up as elevated seabed features of several meters height, with various shapes. a) Kakapo is ovally shaped, Kaka horse-shoe like and Kea presents a ridge-like morphology. b) Bear's Paw stands out as up to 12 m high knoll with close to 400 m in diameter. Moa again is a ridge like feature with steep flanks at the southern end. c) The morphological expression is not as obvious at the three scattered seep occurrences at LM-9.

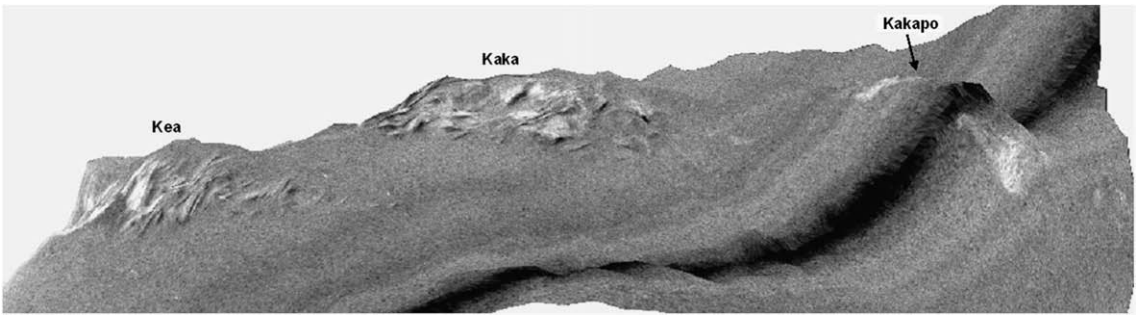

Fig. 12. Three-dimensional view of the Kea, Kaka and Kakapo seep sites, with sidescan backscatter overlain on multibeam swath bathymetry. Note the horseshoe-like shape of the Kaka seep site evident in both the sidescan and multibeam datasets. The width of the Kaka seep site is approximately 300 m (see scale in Fig. 11a).

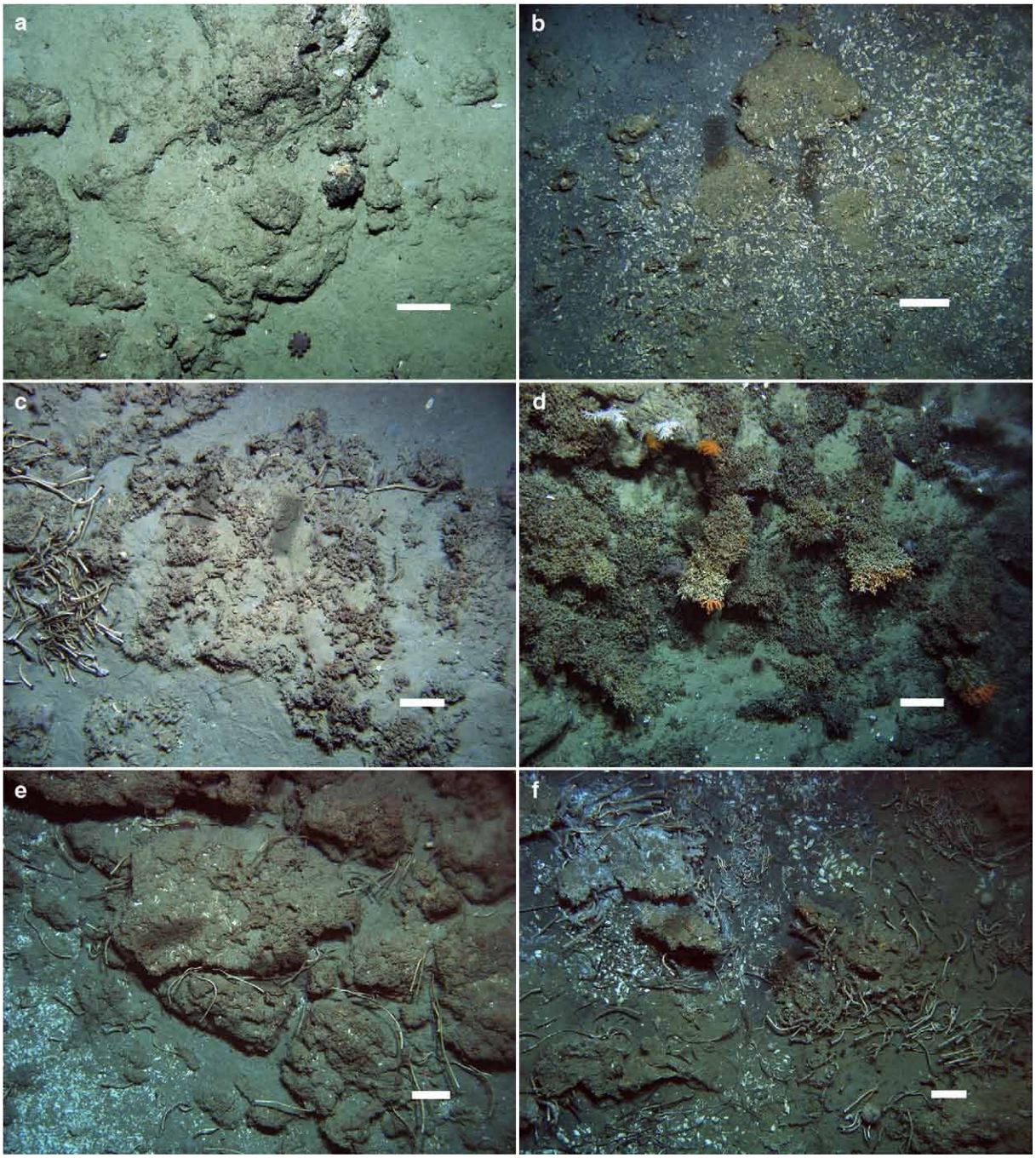

Fig. 13. a) LM-9: carbonate outcrop, low relief. b) Kakapo: Carbonate boulders, sulphidic sediment and *Calyptogena* sp. clam shells c) Kaka: carbonate boulders, *Lamellibrachia* sp. tube worms and mixed low relief epifauna. d) Moa (northwest region): carbonate outcrop with scleractinian corals. e) Moa (southwest region): carbonate outcrop, *Lamellibrachia* sp. tube worms and *Calyptogena* sp. clam shells f) Bear's Paw: Chemoherm, *Lamellibrachia* sp. tube worms, *Calyptogena* sp. clams and shells, hexactinellid sponges, bacterial mat and sulphidic sediment. White scale bars show 20 cm.

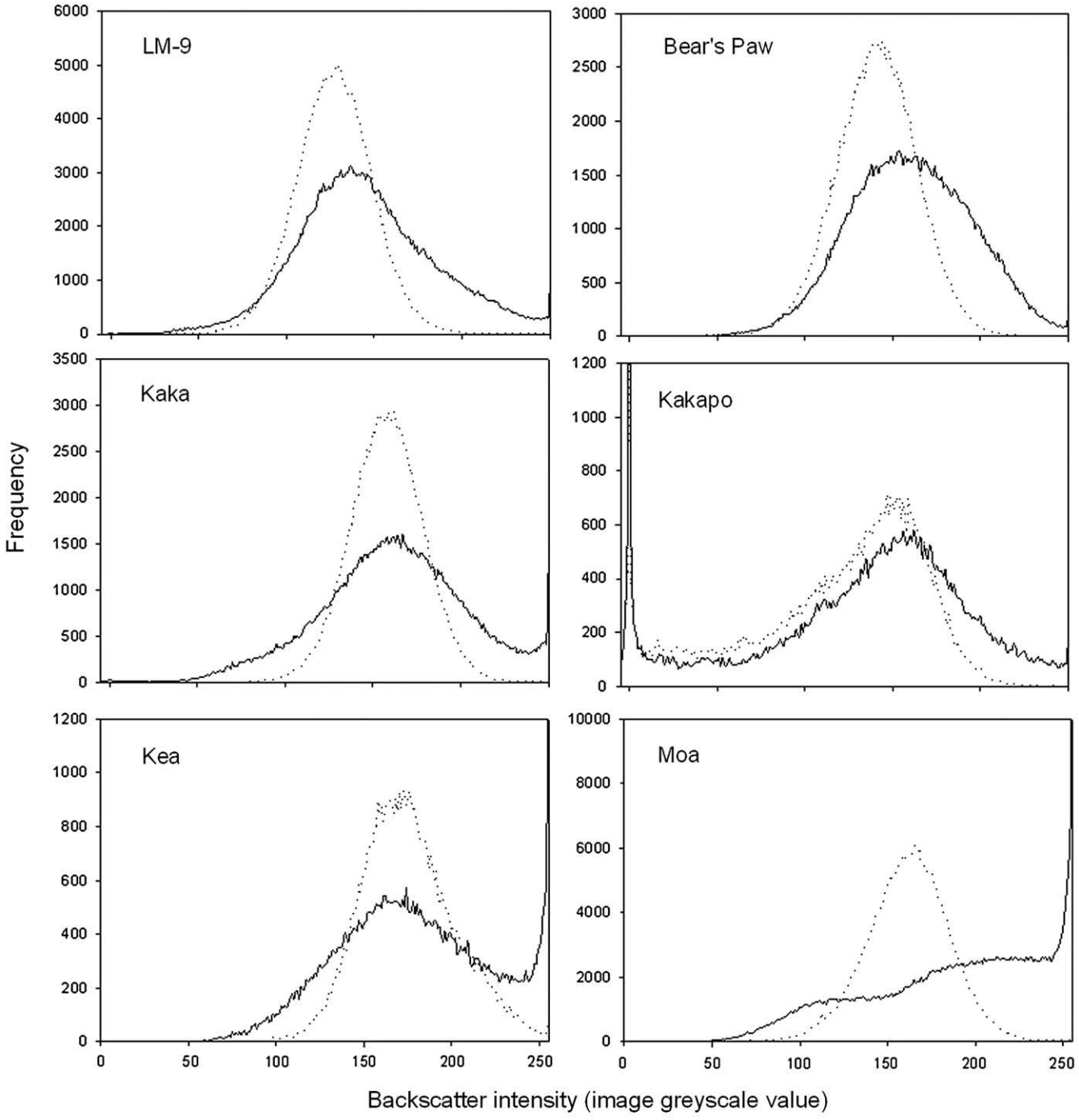

Fig. 14. Sidescan sonar backscatter intensity hiostograms for the 6 seep sites studied on Omakere Ridge. Solid lines show backscatter from seep sites, dotted lines show backscatter from background sediments. Backscatter intensity is represented as greyscale values from mosaiced images of processed sidescan data. Note, image grey scale values range from 0 (black) to 255 (white), higher values corresponding to higher backscatter intensity.

chemoherm extending from its southwestern end. When separate histograms are compared for the reef and the chemoherm components of Moa, the signature of the chemoherm area can be seen to be closer in form to those of the other seep sites whereas the reef histogram is distinctive, with an essentially flat distribution and an extended right tail (Fig. 15).

8. Discussion and conclusions

Seepage of methane from shallow substrata into the overlying water column is apparently a significant process at Omakere Ridge, with seeps developing over a regional gas hydrate accumulation (Henrys et al., 2003; Pecher et al., 2005), evidenced by a BSR in MCS data along the length of Omakere Ridge (Fig. 3). The present data allow us to identify six sites in the Omakere Ridge region where there is evidence of significant methane seepage. By combining high resolution sidescan sonar data with video ground truthing we have been able to describe in some detail their areal extent and geomorphology, and to characterise the biotic assemblages associated with them. These were the primary goals of the study. However, because the chemosynthetic fauna associated with seep sites are dependent, to a greater or lesser extent, on the availability of methane

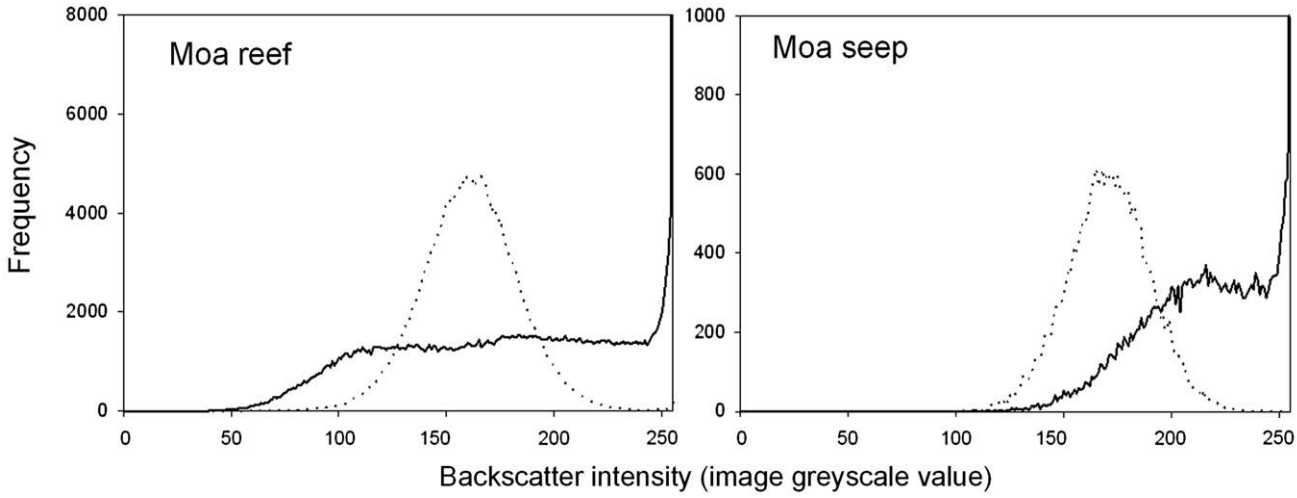

Fig. 15. Sidescan sonar backscatter intensity hiostograms for distinct regions of the Moa study site identified by video ground truthing as being cold water reef (left) and chemoherm (right). Details as for Fig. 14.

or the sulphides generated by the anaerobic oxidation of methane (AOM) (Sibuet and Olu, 1998; Levin, 2005), we can infer from these data that the sites with higher population densities of these live organisms are those where present day seepage is greatest. Furthermore, because another by-product of AOM is the precipitation of authigenic carbonates, we can also infer that where significant carbonate structures exist in combination with evidence of past populations of chemosynthetic taxa (such as the presence of large numbers of vesicomyid clam shells) it is direct evidence of historical seep activity. These inferences allow us to rank the Omakere Ridge sites in estimated order of their present, and past, seep activity with Bear's Paw as the most active, followed by Kea, the southwestern end of Moa, Kaka and Kakapo, LM-9 and finally the main part of Moa, which seems likely to be a relict seep site.

Widespread *Calyptogena* sp. valves and living seep-related biota over the Kea, Kaka and Kakapo sites indicate that methane seepage in this area has been active in the past and remains currently active, despite the absence of acoustic flares in echosounder and sidescan sonar data from SO191. Seep-related biotic assemblages are more developed at the Kea seep (Fig. 7f), which suggests that current methane seepage is greater here than at Kaka and Kakapo.

At LM-9, the presence of *Calyptogena* sp. valves and living seep-related biota across the northern and southern parts of the seep indicates that both have been active in the past and remain currently active but abundances are low. Contrasts in biotic signatures between the two regions (sulphidic sediments and sponges in the south; bacterial mats and corals in the north) may reflect differences in the history of seepage between the two regions but this cannot be diagnosed on the basis of the current dataset.

Very high abundances of living chemosynthetic biota over the Bear's Paw seep indicate that methane seepage at this site has been active in the past and remains currently active, despite the absence of acoustic flares in echosounder and sidescan sonar data from SO191. Although originally identified and named as a single feature, Moa consists of two distinct regions: the main northeastern region of very high relief carbonate rock with corals and other non-seep fauna, and the southwestern chemoherm region which supports abundant chemosynthetic populations (Fig. 9c,d, f). These regions are distinct in both the video ground truth data (Fig. 13d vs Fig. 13e) and in the characteristics of the sidescan sonar image (Figs. 14 and 15). The greater development of carbonate structures in the northeast, combined with the absence of live seep fauna there, fits well with our inferences and indicates that this is an area where there has been active seepage over a long period in the past but that this has now ceased. This indicates that differentiating high-backscatter seabed features in sidescan sonar data as either modern or relict seeps requires judicial analysis and is most effective when supported by visual observations.

The presence of isolated moderate backscatter patches between Bear's Paw and Moa suggest that there is some link between the features. We can speculate that the build up of authigenic carbonates at the Moa site has sealed the initial fluid pathways and that seepage is now displaced to the southwest, or perhaps to the adjacent Bear's Paw site. Alternatively, the locus of methane seepage migrated eastward from the Moa site to the Bear's Paw site. This is supported by the relationship between seep sites to the northwest. Seep-related biotic assemblages are more developed at the Kea and Kaka seeps relative to the Kakapo seep (Fig. 7f). This may be due to seepage having occurred at the Kea and Kaka sites for a longer period of time, thus the locus of seepage may also be migrating to the east in this area. This eastern migration may represent, on an incremental scale, the easterly relocation of the Hikurangi Margin methane seepage system from its ancient position, as recorded in the Miocene uplifted East Coast forearc of New Zealand's eastern North Island, to its current offshore position through tectonic transpression (Campbell et al., 2008).

We have not attempted a statistical analysis of backscatter intensity here; indeed, we have used only image greyscale values as a representation of backscatter strength, rather than any detailed characteristics of the backscatter signal itself (Durand et al., 2002, 2006). Our approach is, thus, little more than a formal illustration of the visual interpretation used during the voyages to detect seep sites. Despite this, the relatively fine distinctions that are apparent between the backscatter characteristics of different substrata across the study area suggests that there is considerable potential to apply more sophisticated techniques using statistical correlations between backscatter characteristics and ground truth observations to predict the nature of seabed features at prospective seep sites.

Acknowledgements

We thank the masters and crews of the RV SONNE and RV TANGAROA. We also thank Henk de Haas and an anonymous reviewer, whose feedback greatly improved the manuscript. AJ publishes with the permission of the Chief Executive Officer, Geoscience Australia. JG wants to thank the EU for financial support via a Marie Curie grant (MOIF-CT-2005-007436). DB was funded by NIWA Capability Fund project CRAR0903.

References

Abrams, M., 2005. Significance of hydrocarbon seepage relative to petroleum generation and entrapment. Mar. Pet. Geol. 22, 457–477.

Barnes, P.M., Lamarche, G., Bialas, J., Henrys, S., Pecher, I., Netzeband, G.L., Greinert, J., Mountjoy, J.J., Pedley, K., Crutchley, G., 2010. Tectonic and Geological Framework for Gas Hydrates and Cold Seeps on the Hikurangi Subduction Margin, New Zealand. Marine Geology 272, 26–48 (this issue).

Campbell, K.A., Francis, D.A., Collins, M., Gregory, M.R., Nelson, C.S., Greinert, J., Aharon, P., 2008. Hydrocarbon seep-carbonates of a Miocene forearc (East Coast Basin), North Island, New Zealand. Sediment. Geol. 204, 83–105.

Durand, S., Le Bel, M., Juniper, S.K., 2002. The use of video surveys, a geographic information system and sonar backscatter data to study faunal community dynamics at Juan de Fuca Ridge hydrothermal vents. Cah. Biol. Mar. 43, 235–240.

Durand, S., Legendre, P., Juniper, S.K., 2006. Sonar backscatter differentiation of dominant macrohabitat types in a hydrothermal vent field. Ecol. Appl. 16, 1421–1435.

Faure, K., Greinert, J., Schneider v.D., J., McGinnis, D.F., Kipfer, R., Linke, P., 2010. Methane seepage along the Hikurangi Margin of New Zealand: Geochemical and physical data from the water column, sea surface and atmosphere. Mar. Geol. 272, 170–188 (this issue).

Greinert, J., Lewis, K., Bialas, J., Pecher, I., Rowden, A., Linke, P., De Batist, M., Bowden, D., Suess, E., 2010. Methane seepage along the Hikurangi Margin, New Zealand: review of studies in 2006 and 2007. Marine Geology 272, 6–25 (this issue).

Henrys, S.A., Ellis, S., Uruski, C., 2003. Conductive heat flow variations from bottom-simulating reflectors on the Hikurangi margin, New Zealand. Geophys. Res. Lett. 30, 1065–1068.

Holland, C.W., Weber, T.C., Etiope, G., 2006. Acoustic scattering from mud volcanoes and carbonate mounds. J. Acoust. Soc. Am. 120, 3553–3565.

Hovland, M., Gudmestad, O.T., 2001. Potential influence of gas hydrates on seabed installations. In: Paull, C.K., Dillon, W.P. (Eds.), Natural Gas Hydrates. Americal Geophysical Union, Geophysical Monograph, vol. 124, pp. 300–309.

Huetten, E., Greinert, J., 2008. Software controlled guidance, recording and post-processing of seafloor observations by ROV and other towed devices: the software package OFOP. Geophysical Research Abstracts, 10. EGU2008-A-03088.

Judd, A.G., Hovland, M., 2007. Seabed Fluid Flow: The Impact on Geology, Biology and the Marine Environment. Cambridge University Press, New York. 475 pp.

Kennicut, M.C., Brooks, J.M., Bidigare, R.R., Fay, R.R., Wade, T.L., McDonald, T.J., 1985. Vent type taxa in a hydrocarbon seep region on the Louisiana Slope. Nature 317, 351–353.

Klaucke, I., Sahling, H., Bürk, D., Weinrebe, W., Bohrmann, G., 2005. Mapping deep-water gas emissions with sidescan sonar. EOS 86, 341–346.

Klaucke, I., Sahling, H., Weinrebe, W., Blinova, V., Bürk, D., Lursmanashivili, N., Bohrmann, G., 2006. Acoustic investigation of cold seeps offshore Georgia, eastern Black Sea. Mar. Geol. 231, 51–67.

Kvenvolden, K.A., 1988. Methane hydrate—a major reservoir or carbon in the shallow geosphere? Chem. Geol. 71, 41–51.

Kvenvolden, K.A., Rogers, B.W., 2005. Gaia's breath—global methane exhalations. Mar. Pet. Geol. 22, 579–590.

Le Bas, T.P., Mason, D.C., Millard, N.W., 1995. TOBI image processing—the state of the art. IEEE J. Oceanic Eng. 20, 85–93.

Levin, L.A., 2005. Ecology of cold seep sediments: interactions of fauna with flow, chemistry and microbes. Oceanogr. Mar. Biol.: Annu. Rev. 43, 1–46.

Lewis, K.B., Marshall, B.A., 1996. Seep faunas and other indicators of methane-rich dewatering on New Zealand convergent margins. N.Z. J. Geol. Geophys. 39, 181–200.

Max, M.D., 2000. Hydrate resource, methane fuel, and a gas-based economy? In: Max, M.D. (Ed.), Natural Gas Hydrates in Oceanic and Permafrost Environments. Kluwer Academic Publishers, Dordrecht, pp. 361–370.

McGinnis, D.F., Greinert, J., Artemov, Y., Beaubien, S.E., Wuest, A., 2006. Fate of rising methane bubbles in stratified waters: how much methane reaches the atmosphere? J. Geophys. Res., Oceans 111 (C09007). doi:10.1029/2005JC003183.

Naudts, L., Greinert, J., Artemov, Y., Beaubien, S.E., Borowski, C., De Batist, M., 2008. Anomalous sea-floor backscatter patterns in methane venting areas, Dnepr paleo-delta, NW Black Sea. Mar. Geol 251, 253–267.

Netzeband, G.L., Krabbenhoeft, A., Zillmer, M., Petersen, C.J., Papenberg, C., Bialas, J., 2010. The structures beneath submarine methane seeps: seismic evidence from Opouawe Bank, Hikurangi Margin, New Zealand. Marine Geology 272, 59–70 (this issue).

Niemann, H., Elvert, M., Hovland, M., Orcutt, B., Judd, A., Suck, I., Gutt, J., Joye, S., Damm, E., Finster, K., Boetius, A., 2005. Methane emission and consumption at a North Sea gas seep (Tommeliten area). Biogeosciences 2, 335–351.

Orange, D.L., Yun, J., Maher, N., Barry, J., Greene, G., 2002. Tracking California seafloor seeps with bathymetry, backscatter and ROVs. Cont. Shelf Res. 22, 2273–2290.

Pecher, I.A., Henrys, S.A., Ellis, S., Chiswell, S.M., Kukowski, N., 2005. Erosion of the seafloor at the top of the gas hydrate stability zone on the Hikurangi Margin, New Zealand. Geophys. Res. Lett. 32 (L24603). doi:10.1029/2005GL024687.

Rollet, N., Logan, G.A., Kennard, J.M., O, Brien, P., Jones, A.T., Sexton, M., 2006. Characterisation and correlation of active hydrocarbon seepage using geophysical data sets: an example from the tropical, carbonate Yampi Shelf, Northwest Australia. Mar. Pet. Geol. 23, 145–164.

Schmale, O., Greinert, J., Rehder, G., 2005. Methane emission from high-intensity marine gas seeps in the in the Black Sea into the atmosphere. Geophys. Res. Lett. 32 (L07609). doi:10.1029/2004GL021138.

Sibuet, M., Olu, K., 1998. Biogeography, biodiversity and fluid dependence of deep-sea cold-seep communities at active and passive margins. Deep-sea Res., Part 2, Top. Stud. Oceanogr. 45, 517–567.

Wilson, R.D., Monaghan, P.H., Osanik, A., Price, L.C., Rogers, M.A., 1974. Natural marine oil seepage. Science 184, 857–865.